Proceedings of the 7th Annual ISC Graduate Research Symposium
ISC-GRS 2013
April 24, 2013, Rolla, Missouri

RELIABILITY ANALYSIS FOR HYDROKINETIC TURBINE BLADES UNDER RANDOM RIVER VELOCITY FIELD

Zhen Hu
Department of Mechanical and Aerospace Engineering
Missouri University of Science and Technology Rolla, MO, USA, 65401

Xiaoping Du
Department of Mechanical and Aerospace Engineering
Missouri University of Science and Technology Rolla, MO, USA, 65401

ABSTRACT

Hydrokinetic energy is one of the renewable energies that gain much global attention recent years. Hydrokinetic turbine is used to extract energy from the flowing river water. Reliability is a critical issue that needs to be addressed during the development process of hydrokinetic turbine systems. In this work, a new reliability analysis method is proposed for the hydrokinetic turbine blades under random river velocity field. A river velocity field is established first. The critical working position of turbine blades is then identified by using the blade element momentum (BEM) theory. The river velocity is modeled as a random field with variations and correlations both in spatial and temporal domains. The time-dependent characteristics of river flow loading are captured by time series models. The effect of time-dependent river velocity field on the reliability of turbine blades is investigated. The proposed method is compared with the Monte Carlo Simulation (MCS) in the case study. The results demonstrate that the developed method can predict the time-dependent reliability of turbine blades efficiently and accurately.

1. INTRODUCTION

With the world's increasing demand in carbon-free energy, renewable energy resources are gaining special attentions recent years [1-4]. The commonly used renewable energy sources include sunlight, wind, rain, tides, waves, geothermal heat, and so on. Amongst these renewable energies, hydrokinetic energy extracted from flowing water is one of the most sustainable ones. The hydrokinetic energy is different from the hydro power energy captured by conventional hydraulics turbines [5-9]. Hydrokinetic turbines used to extract hydrokinetic energy are zero-headed. They have similar working principles as wind turbines, which convert the hydrokinetic power into mechanical power in the form of rotating blades. Unlike hydraulics turbines, the hydrokinetic turbine is portable and has low initial construction cost. Hydrokinetic turbines can be classified into two categories according to their system configurations. They are the vertical axis turbines and the horizontal axis turbines as shown in Fig. 1. During the developing process of horizontal axis hydrokinetic turbines, reliability is a critical issue that needs to be addressed because it is directly related to the system lifetime cost and the commercialization of the system. Since the hydrokinetic turbine blade is the most vital element of the turbine system, its safety is always a special focus.

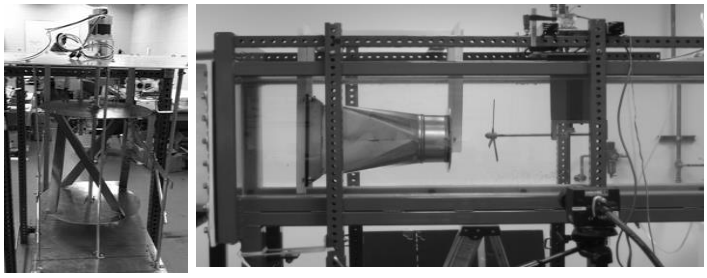

(a). Vertical axis (b). Horizontal axis

Fig. 1. Two configurations of hydrokinetic turbine system

In the past decades, many reliability analysis methods have been developed for wind and hydrokinetic turbine blades. For instance, several reliability analysis methods have been developed for the wind turbine blades by Ronold [10], Agarwal [11], and Manuel [12, 13]. Even though the wind turbine and the hydrokinetic turbine share similar working principles, the reliability analysis methods for wind turbine blades cannot be applied to the hydrokinetic turbine blades directly as the working environments are different. To overcome this, Hu and Du [14] proposed a time-dependent reliability analysis method for hydrokinetic turbine blades by considering the time-dependent characteristics of river climate. Val and Chernin [15] developed a reliability analysis method to account for the uncertainties in the blade resistance and water speed. A simulation based reliability analysis method is then developed in [16] to investigate the uncertainties in the composite material of the turbine blade. Delorm and Zappala, et. al. [17] compared the reliability of different hydrokinetic turbine systems and shown that the hydrokinetic turbine devices have a much lower reliability than wind turbines of comparable size. The above reviewed reliability analysis methods are capable to approximate the reliability of wind or hydrokinetic turbine systems from different aspects under certain assumptions. These methods, however, have some drawbacks. One of the main drawbacks is that the wind or river velocity is usually modeled as a random variable and that the uncertainties in the spatial and temporal domains are not considered.

In practical, it is more reasonable to express the river velocity as a random field rather than a random variable. A random field is able to consider the dependency as well as variation of a variable over time and space simultaneously. Recently, some researchers begin to pay their attentions to the modeling of wind climate as a random field. For example,

Manuel, et. al [18, 19] performed stochastic simulations for the wind field by modeling the inflow turbulence as a random field. Choi et.al. [20] used a random field model to describe the time-varying fluctuating wind speed. Law and Bu [21] employed an ergodic multivariate stochastic process to simulate the fluctuating wind velocity. In this work, the river velocity, which governs the response of turbine blades, is also modeled as a random field.

When both uncertainties and correlations in space and time domains are considered, current reliability analysis methods are inapplicable anymore. Most of current methods account for the uncertainties and correlations either in the time domain or in the space domain. For instance, time-dependent reliability analysis methods have been investigated intensively by using the extreme response method [22-24], the sampling method [25-27], and the upcrossing rate method [14, 28-30]. These methods consider the correlations in the time domain rather than in the space domain. The reliability analysis methods developed by Xi [31] and Missoum [32, 33] concentrated on the correlations of random field in spatial region while the dependencies at time instants were ignored. In this work, a recently developed sampling reliability analysis method is integrated with the proper orthogonal decomposition (POD) method to approximate the reliability of hydrokinetic turbine blades under time-dependent random river velocity field.

The reminder of this work is given as follows. In Section 2, the model of river velocity field is discussed. Following that, the critical working position of the turbine blade is identified in Section 3. Section 4 gives the random field model for the river velocity at the critical working position. The reliability analysis method for the turbine blade under random velocity field is presented in Section 5. A study example is given in Section 6 and conclusions are made in Section 7.

2. RIVER VELOCITY FIELD MODEL

The river velocity field model is vital for the performance analysis of hydrokinetic turbine system as it governs the response of the system. Define the river velocity field in the rotating plane of hydrokinetic turbine blades as $v(x, y)$. By making reference to the wind field model [34], we can present $v(x, y)$ as:

$$v(x, y) = v_s(x, y) + v_t(x, y) \tag{1}$$

where $v_s(x, y)$ is vertical river shear velocity and $v_t(x, y)$ is the tower shadow.

Eq. (1) can be modeled by the following three river phenomena.

a) River velocity at the hub

For the modeling of river velocity field, the turbine hub is usually used as the origin of the coordinate system. At the hub, we have $x = y = 0$. Let the river velocity at the hub be v_h, $v_s(x, y)$ and $v_t(x, y)$ can then be presented as functions of v_h, *x*, and *y*.

b) Vertical river shear $v_s(x, y)$

The river velocity profile of the river cross section is very complicated. It is related to many factors of the river environment, such as the roughness and slope of the river bed, the shape of river bank, and so on [35]. Since for wide rivers the depth is very small when compared with its wide, the velocity profile of the rotation plane can be assumed to be uniform in the horizontal direction. We therefore only consider the shear velocity of the vertical profile. As indicated in Fig. 2, let the distance from the hub center of hydrokinetic turbine to the river bed be *H*, the shear velocity at *H+y* is then given by

$$v_s(x, y) = v_h\left(\frac{H + y}{H}\right)^a \tag{2}$$

where a is the empirical river shear exponent.

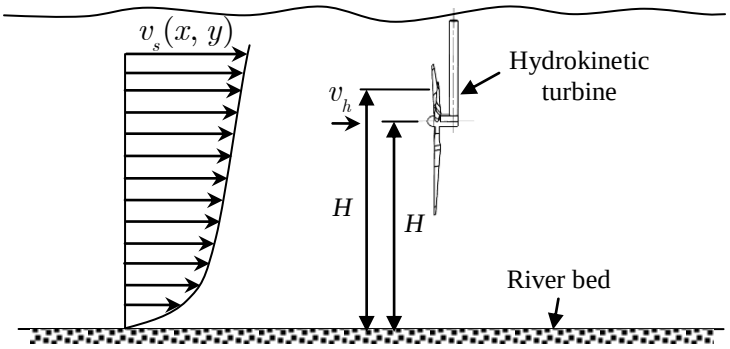

Fig. 2. Illustration of the shear river velocity

c) Tower shadow

The effect of hydrokinetic turbine support shaft on the river velocity distribution is called the tower shodow. Similar to the wind field problem, herein, the tower shadow model developed by Dolan and Lehn [36] is employed. For a hydrokinetic turbine configuration given in Fig. 3, the tower shadow is given by

$$v_t(x, y) = v_h\eta\left(\frac{D}{2}\right)^2 \frac{x^2 - d^2}{(x^2 + d^2)^2} \tag{3}$$

$$\eta = 1 + \frac{a(a-1)R^2}{8H^2} \tag{4}$$

where D, x, and d are dimensional parameters given in Fig. 3.

For a given radius *r*, $x = r\cos(\theta)$, and Eq. (3) is then transformed as follows:

$$v_t(x, y) = v_h\eta\left(\frac{D}{2}\right)^2 \frac{r^2\cos^2(\theta) - d^2}{(r^2\cos^2(\theta) + d^2)^2} \tag{5}$$

Converting the coordinate *y* into *r* and θ and plugging Eqs. (2) and (5) into Eq. (1), we have

$$v(r,\theta) = v_h\left(\frac{H + r\sin(\theta)}{H}\right)^a + v_h\left(1 + \frac{a(a-1)R^2}{8H^2}\right)\left(\frac{D}{2}\right)^2 \frac{r^2\cos^2(\theta) - d^2}{(r^2\cos^2(\theta) + d^2)^2} \quad (6)$$

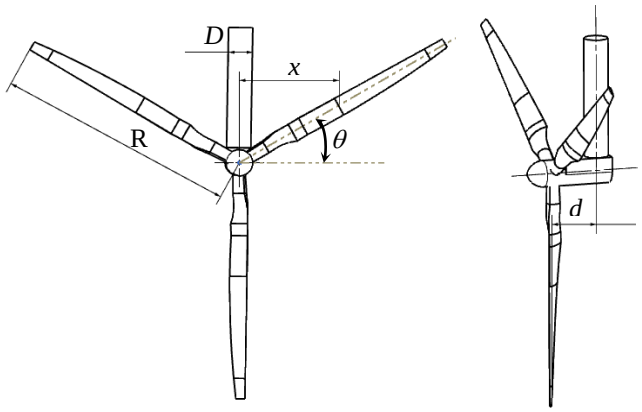

Fig. 3. Illustration of dimensions of hydrokinetic turbine

Considering that the effect of the tower shadow on the velocity distribution below the horizontal line is minor, we have $v_t(x, y) = 0$ for $180^\circ \le \theta \le 360^\circ$. Eq. (6) is then written as

$$v(r,\theta) = \begin{cases} v_h\left(\frac{H + r\sin(\theta)}{H}\right)^a + v_h\left(1 + \frac{a(a-1)R^2}{8H^2}\right) \\ \times\left(\frac{D}{2}\right)^2 \frac{r^2\cos^2(\theta) - d^2}{(r^2\cos^2(\theta) + d^2)^2}, \ 0^o \le \theta \le 180^o \\ v_h\left(\frac{H + r\sin(\theta)}{H}\right)^a, \text{otherwise} \end{cases} \quad (7)$$

Fig. 4 shows a simulated example of the river velocity field over the rotational plane of hydrokinetic turbine.

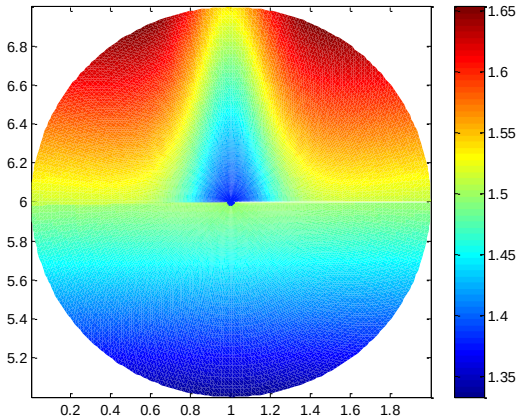

Fig. 4. River flow velocity field over the rotation plane of hydrokinetic turbine

It should be noted that the river field model is established according to the wind field model. It might be replaced with more accurate models in the future. The reliability analysis method presented in this work can be still used. In the subsequent section, we will discuss how the velocity field is used to identify the critial working position of hydrokinetic turbine.

3. IDENTIFICATION OF CRITICAL WORKING POSITION

3.1. Local loads analysis

The local loads of hydrokinetic turbine blades depend on the local river velocity, geometry of hydrokinetic turbine blades, and many other factors. To accurately analyze the local loads at different stations of the turbine blade, the three dimensional computational fulid dynamics (CFD) simulations should be performed [37]. The CFD simulation, however, is very compuationally expensive. In liue of using CFD, the blade element momentum (BEM) theory proposed by Glauert in 1935 has been widely used by many engineers and researchers. Even though the accuracy of BEM is not as good as that of CFD, the efficiency of BEM is much better. In this work, the BEM theory is employed to approximate the local hydrodynamic loads on the turbine blade.

For a turbine blade at the position of angle θ as shown in Fig. 5, the edgewise force p_T and the flapwise force p_N on the station *r* of the turbine blade can be approximated using BEM. To compute p_T and p_N for station *r* at angle θ, the flow dynamic loads on the hydrofoil are analyzed first. As shown in Fig. 6, the relative velocity $v_{rel}(r,\theta)$ acting on the hydrofoil is given by

$$v_{rel}(r,\theta) = \sqrt{[v(r,\theta)(1-\delta)]^2 + [\omega r(1+\delta')]^2} \quad (8)$$

where ω is the angular velocity of the turbine blade, δ and δ' are axial induction factor and tangential induction factor, respectively. The axial and tangential induction factors can be obtained by following an iteration algorithm given in [37]. To consider the effect of hub and make BEM more accurate, Prandtl and Glauert made corrections to δ and δ' [38]. Since BEM is not the concentration of this work, we do not discuss details. More about BEM can be found in [37].

Based on the force analysis given in Figs. 5 and 6, p_T and p_N can be computed by [37]

$$p_N(r,\theta) = L_1(r,\theta)\cos(\gamma) + D_1(r,\theta)\sin(\gamma) \quad (9)$$

$$p_T(r,\theta) = L_1(r,\theta)\sin(\gamma) - D_1(r,\theta)\cos(\gamma) \quad (10)$$

in which $L_1(r,\theta)$ and $D_1(r,\theta)$ are local lift and drag forces on station *r* of the turbine blade and are given by

$$L_1(r,\theta) = \frac{1}{2}\rho v_{rel}^2(r,\theta)c(r)C_l \quad (11)$$

$$D_1(r,\theta)=\frac{1}{2}\rho v_{rel}^2(r,\theta)c(r)C_d \tag{12}$$

and

$$\tan\gamma=\frac{v(r,\theta)(1-\delta)}{\omega r(1+\delta')} \tag{13}$$

where $c(r)$ is the chord length at station *r* of the turbine blade, ρ is the density of water, and C_l and C_d are the lift and drag coefficients of the hydrofoil, respectively. The lift and drag coefficients of the hydrofoil can be computed based on the angle of attack α, which is given by

$$\alpha=\gamma-\varsigma \tag{14}$$

in which ς is the local pitch.

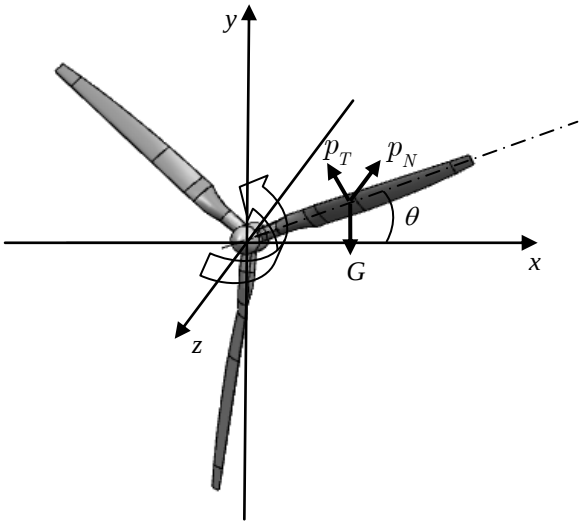

Fig. 5. Forces on a hydrokinetic turbine blade

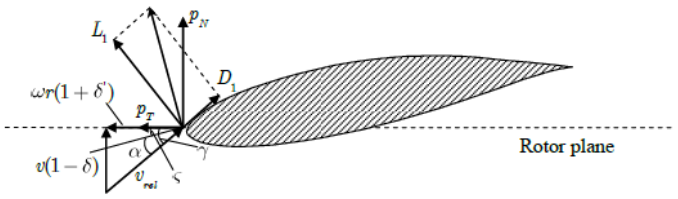

Fig. 6. Local loads on the turbine blade

With expressions about the local loads on the turbine blade, we then discuss how the loads are applied to compute the moments of the turbine blade.

3.2. Moments analysis

According to the forces analysis in the last section, there are three kinds of moments on the turbine blade. They are the edgewise moment M_1 generated from the edgewise force p_T, the moment comes from the gravity force G, and the flapwise bending moment M_2 due to the flapwise force p_N. To approximate the these moments, the turbine blade is divided into n_r stations along the radial direction with the radius at station *i* be $r_i=r_{root}+\frac{i(R-r_{root})}{n_r}$, $i=1,2,\cdots,n_r$, where r_{root} stands for the root of the turbine blade.

Based on the discretion and the assumption of linear variation between two stations, the edgewise and flapwise moments are computed as below [37]:

$$M_{j,i}=\frac{1}{3}A_{j,i}(r_{i+1}^3-r_i^3)+\frac{1}{2}B_{j,i}(r_{i+1}^2-r_i^3),\quad j=1,2 \text{ and } i=1,2,\cdots,n_r-1 \tag{15}$$

where

$$A_{1,i}=\frac{p_T(r_{i+1},\theta)-p_T(r_i,\theta)}{r_{i+1}-r_i} \tag{16}$$

$$B_{1,i}=\frac{p_T(r_i,\theta)r_{i+1}-p_T(r_{i+1},\theta)r_i}{r_{i+1}-r_i} \tag{17}$$

$$A_{2,i}=\frac{p_N(r_{i+1},\theta)-p_N(r_i,\theta)}{r_{i+1}-r_i} \tag{18}$$

and

$$B_{2,i}=\frac{p_N(r_i,\theta)r_{i+1}-p_N(r_{i+1},\theta)r_i}{r_{i+1}-r_i} \tag{19}$$

Once the moments at different stations are available, M_1 and M_2 are computed by

$$M_j=\sum_{i=1}^{n_r-1}M_{j,i},\ j=1,2 \tag{20}$$

The total moment on the turbine blade is then given by

$$M_{total}(\theta)=\sqrt{(M_1-Gr_c\cos(\theta))^2+M_2^2} \tag{21}$$

where r_c is the centroid of the turbine blade.

It can be seen from Eq. (21) that the total moment of the turbine blade is a function of the position angle θ. There exists a critical working position such that the total moment on the turbine blade is maximal. At the critical position, it is possible that the turbine blade has the highest probability of failure.

3.3. Identification of critical working position

With the total moment given in Eq. (21), the critical working position of the turbine blade is identified by solving the following optimization model:

$$\begin{cases}\max\ M_{total}(\theta)\\ \text{Subject to:}\\ M_{total}(\theta)=\sqrt{(M_1-Gr_c\cos(\theta))^2+M_2^2}\\ 0\le\theta\le 2\pi\end{cases} \tag{22}$$

Let the solution from Eq. (22) be θ^*, the velocity profile on the turbine blade at the critical working postion can then be computed by

$$v(r,\theta^*) = v_h\left(\frac{H + r\sin(\theta^*)}{H}\right)^a + v_h\left(1 + \frac{a(a-1)R^2}{8H^2}\right)\left(\frac{D}{2}\right)^2 \frac{r^2\cos^2(\theta^*) - d^2}{(r^2\cos^2(\theta^*) + d^2)^2} \quad (23)$$

Plugging the discretized radii $r_i = r_{root} + \frac{i(R - r_{root})}{n_r}, i = 1, 2, \cdots, n_r$ into Eq. (23) and combining Eq. (23) and Eqs. (9), (10), and (15), we have the moments at different stations of the critical working position.

4. CONSTRUCTION OF RANDOM RIVER FLOW FIELD AT THE CRITICAL POSITION

The above analyses are in the deterministic form, in which the fluctuations of river velocity over time and space have not been considered. By introducing the turbulence part to the river velocity model, the river velocity profile on the turbine blade at the critial position becomes

$$v_c(r,t) = v(r,\theta^*) + \tilde{v}(r,t) \quad (24)$$

in which $v(r,\theta^*)$ is the mean value of the velocity profile obtained from Eq. (23) and $\tilde{v}(r,t)$ is a random field used to represent the fluctuation of the river velocity.

As $\tilde{v}(r,t)$ is a random field, $v_c(r,t)$ is also a random field. In the past decades, many researchers have made their contributions to the modeling of random field. Amongst the developed methods, the most commonly used method include the polynomial chaos expansion method [16, 39], the shape function method [40], the optimal linear estimation method [41], the Karhunen-Loève expansion [42-45], the midpoint method [46], and the expansion optimal linear estimation method [41]. A detailed analysis and comparison about these modeling methods for the random field can be found in [47]. The above mentioned methods assume that the information of a random field, such as its mean, standard deviation, and covariance functions are known. In practical, the information is usually unavailable. The proper orthogonal decomposition (POD) method has been recently introduced to the modeling of random field based on experimental data by Koizumi [55], Kopp [58], Missoum [32, 33], Manuel [48, 49], and Youn [31]. The POD method finds the most appropriate sequence of orthogonal functions to approximate the random field collected from data in time sequence.

With the POD method, the random filed $v_c(r,t)$ is approximated as

$$v_c(r,t) \approx v(r,\theta^*) + \sum_{j=1}^{n_f} q_j(t)\phi_j(r) \quad (25)$$

in which n_f is the number of important features used to approximate the random field, $\phi_j(r)$ is the *j*-th important feature of the random field, and $q_j(t)$ is the coefficient of *j*-th important feature.

The correlation of the random field over the space domain is captured by the important features $\phi_j(r)$ and the correlation in time domain is indicated by the time-dependent coefficients $q_j(t)$. The randomness of the random field is also presented in $q_j(t)$. To represent the randomness and correlation in time domain, $q_j(t)$ are usually given in time series models as below

$$q_j(t_i) - \mu_{q_j} = \gamma_1(q_j(t_{i-1}) - \mu_{q_j}) + \gamma_2(q_j(t_{i-2}) - \mu_{q_j}) + \cdots + \gamma_p(q_j(t_{i-p}) - \mu_{q_j}) + \varepsilon_j \quad (26)$$

where μ_{q_j} is the mean value of $q_j(t)$, γ_i, where $i = 1, 2, \cdots, p$, is the coefficients of time series model, p is the order of the time series, and ε_j is a Gaussian white noise used to represent the randomness of the model.

Based on the model of time series given in Eq. (26), the mean, standard deviation, auto-correlation, and partial correlation functions of the time series models can be computed using the Yule-Walker method, the Burg method, or the covariance method [50]. Fig. 7 shows a simulated random river velocity field on the turbine blade.

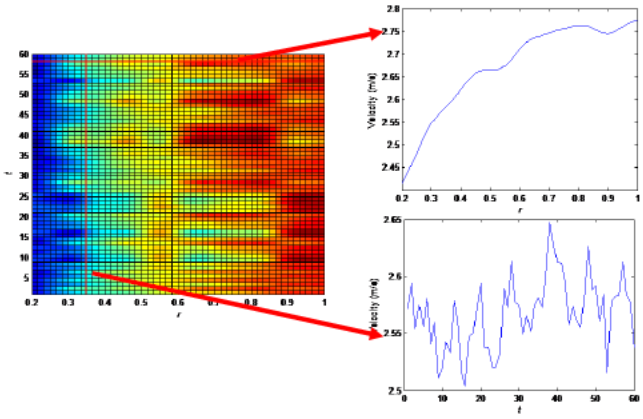

Fig. 7. Example of the random river velocity field on the turbine blade

The figure indicates that the random field model is able to represent the randomness and correlation in time and space domains simultaneously. As the random field model given in Eq. (25) has considered the correlations in both time and space domains, the velocity profile is different at different time instants. We call this kind of random field as the time-dependent random field.

5. RELIABILITY ANALYSIS UNDER TIME-DEPENDENT RANDOM FIELD

In this section, we first analyze the uncertainties existed in the working environment of turbine blade. We then give the limit-

state function of the turbine blade. Based on the uncertainty analysis and limit-state function, the reliability analysis method is developed.

5.1. Uncertainty analysis

There are mainly two kinds of uncertainties that may affect the performance of the turbine blade. They are the random velocity field as discussed in Section 4 and the uncertainties presented in the material properties.

The difference between these two kinds of uncertainties is the random velocity field changes with time while the uncertaintis of material properties do not vary with time. Herein, the time-invariant uncertainties are presented as $\mathbf{X} = [X_1, X_2, \cdots, X_{n_{it}}]$, where n_{it} indicates the number of time-invariant uncertainties or random variables. Assume that the random velocity field is approximated using the first n_f important features, there are totally $n_{it} + n_f$ uncertain sources involved in the turbine blade working environment.

5.2. Limit-state function

A failure of the turbine blade is defined as the event that the maximum stress on the turbine blade is larger than the strength of the material. Let the maximum stress on the turbine blade be $S_{\max}(v_c(r, t), \mathbf{X})$ and the strength of the material be X_1, the limit-state function of the turbine blade is then given by

$$g(v_c(r, t), \mathbf{X}) = S_{\max}(v_c(r, t), \mathbf{X}) - X_1 \tag{27}$$

The safety state of the turbine blade is then defined as

$$\text{state} = \begin{cases} \text{safe, if } g(v_c(r, t), \mathbf{X}) \le 0 \\ \text{fail, otherwise} \end{cases} \tag{28}$$

The maximum stress $S_{\max}$ given in Eq. (27) can be computed either in analytical way or in the simulation way, such as Finite Element Analysis (FEA) method. In this work, the FEA method was employed.

5.3. Reliability analysis for turbine blade under time-dependent random velocity field

Since the random velocity field $v_c(r, t)$ varies with time, the reliability of the turbine blade is also time-variant. For the time-dependent reliability of the turbine blade, the reliability will decrease with the increase of the time interval. The time-dependent probability of failure of the turbine blade is defined as the probability that the turbine blade goes into the failure region over a spefic time interval.

Let the time-dependent probability of failure be $p_f(t_0, t_s)$, which is given by

$$p_f(t_0, t_s) = \Pr\{g(v_c(r, \tau), \mathbf{X}) > 0, \exists \tau \in [t_0, t_s]\} \tag{29}$$

where t_0 and t_s are the initial and end time instants of the time interval.

For approximating the time-dependent probability of failure, many approaches have been proposed in the past decades [14, 22-30]. A detailed review about these method is available in [51]. Even if the available methods are able to approximate the time-dependent probability of failure under different kinds of situations, they still have some limitations. In this paper, we extend a recently developed sampling approach to the reliability analysis under time-dependent random velocity field [51].

Assume that the time-dependent coefficients $q_j(t)$ of random field $v_c(r, t)$ are modeled as stationary time series models, to apply the sampling approach, we first transform $\mathbf{q}(t) = [q_1(t), q_2(t), \cdots, q_{n_f}(t)]$ and $\mathbf{X}$ into $\mathbf{U}_{\mathbf{q}}(t)$ and $\mathbf{U}_{\mathbf{X}}$ at any time instant *t* over time interval $[t_0, t_s]$, where $\mathbf{U}_{\mathbf{q}}(t)$ and $\mathbf{U}_{\mathbf{X}}$ are corresponding standard Gaussian random variables. After the transformation, Eq. (31) becomes:

$$p_f(t_0, t_s) = \Pr\{g(T(\mathbf{U}_{\mathbf{q}}(t)), T(\mathbf{U}_{\mathbf{X}})) > 0, \exists \tau \in [t_0, t_s]\} \tag{30}$$

where $T(\cdot)$ stands for transforming operator.

With the transformed limit-state function, at a given time instant *t*, the most probable point (MPP) is then identified by solving the following optimization model:

$$\begin{cases} \min\ \beta(t) = \left\|\mathbf{u}(t)\right\| \\ \mathbf{u}(t) = [\mathbf{u}_{\mathbf{q}}(t), \mathbf{u}_{\mathbf{X}}] \\ g(T(\mathbf{u}_{\mathbf{q}}(t)), T(\mathbf{u}_{\mathbf{X}})) \le 0 \end{cases} \tag{31}$$

Once the MPP $\mathbf{u}^*(t)$ is available, the time-dependent probability of failure given in Eq. (30) is equivalent to the following probability:

$$p_f(t_0, t_s) = \Pr\{L(\tau) = \boldsymbol{\alpha}(\tau)\mathbf{U}^T(\tau) > \beta(\tau), \exists \tau \in [t_0, t_s]\} \tag{32}$$

where

$$\boldsymbol{\alpha}(t) = \frac{\mathbf{u}^*(t)}{\left\|\mathbf{u}^*(t)\right\|} \tag{33}$$

and

$$\beta(t) = \left\|\mathbf{u}^*(t)\right\| \tag{34}$$

in which $\|\cdot\|$ stands for the determinant.

For approximating the probability given in Eq. (32), $L(t)$ is then expanded using the Orthogonal Series Expansion (OSE) method as [51]

$$L(t) \approx \sum_{i=0}^{M} \sqrt{\lambda_i}\xi_i \left(\sum_{j=0}^{M} P_j^i h_j(t)\right) \tag{35}$$

where M is the expansion order, $h_j(t)$ is the *j*-th order Legendre polynomials [52], ξ_i are identical independent

standard Gaussan random varaibles, λ_i and P_j^i are the *i*-th eigenvalue and the *j*-th element of *i*-th column of the eigenvector associated with the following covariance matrix:

$$\sum_{M\times M}=\begin{bmatrix} C_{11} & C_{12} & \cdots & C_{1M} \\ C_{21} & C_{22} & \cdots & C_{2M} \\ \vdots & \vdots & \ddots & \vdots \\ C_{M1} & C_{M2} & \cdots & C_{MM} \end{bmatrix} \tag{36}$$

in which

$$C_{ij}=\int_{t_0}^{t_s}\int_{t_0}^{t_s}\rho_{LL}(t,t')h_i(t)h_j(t')dtdt' \tag{37}$$

Typically there is no explicit solution available for the double integral given in Eq. (37). To solve this integral equation, numerical integration method should be employed. For example, the Gaussian-Legendre Quadrature method, which transforms the integral into summation of functions at Gaussian points, can be used.

The $\rho_{LL}(t,t')$ given in Eq. (37) stands for the correlation coefficient of $L(t)$ at two time instants t and t'. It is given by

$$\rho_{LL}(t,t')=\boldsymbol{\alpha}(t)\mathbf{C}(t,t')\boldsymbol{\alpha}^T(t') \tag{38}$$

where

$$\mathbf{C}(t,t')=\begin{bmatrix} 1 & 0 & 0 & \cdots & \cdots & 0 \\ 0 & \ddots & 0 & \vdots & 0 & 0 \\ 0 & \cdots & 1 & 0 & \vdots & \vdots \\ \vdots & 0 & 0 & \rho_1(t,t') & 0 & 0 \\ 0 & \vdots & \vdots & 0 & \ddots & 0 \\ 0 & 0 & 0 & \cdots & \cdots & \rho_{n_f}(t,t') \end{bmatrix} \tag{39}$$

in which $\rho_i(t,t')$ is the auto-correlation function of *i*-th time series model $q_i(t)$.

With the Yule-Walker method, the auto-correlation function of $q_i(t)$ can be obtained by solving the following equation iteratively:

$$\begin{bmatrix} \rho_1 \\ \rho_2 \\ \vdots \\ \rho_p \end{bmatrix}=\begin{bmatrix} 1 & \rho_1 & \cdots & \rho_{p-1} \\ \rho_1 & 1 & \cdots & \rho_{p-2} \\ \vdots & \vdots & \ddots & \vdots \\ \rho_{p-1} & \rho_{p-1} & \cdots & 1 \end{bmatrix}\begin{bmatrix} \gamma_1 \\ \gamma_2 \\ \vdots \\ \gamma_p \end{bmatrix} \tag{40}$$

Based on the expansion model given in Eq. (35), N_s samples are generated for each standard Gaussian random variable ξ_i and the time interval $[t_0, t_s]$ is divided into N_T time instants. Plugging the N_T time instants and N_s samples of ξ_i into Eq. (35), we therefore obtain a $N_s\times N_T$ sample matrix for $L(t)$ over time interval $[t_0, t_s]$ [51]. Let the generated sample matrix be $\tilde{L}_{N_s\times N_T}$ with element $l(i,j)$ be the *i*-th sample at *j*-th time instant, we then obtain the extreme value samples of $L(t)$ as follows:

$$l_{\max}(i)=\max\{l(i,1),l(i,2),\cdots,l(i,N_T)\} \tag{41}$$

With the extreme value samples of $L(t)$, the time-dependent probability of failure given in Eq. (29) and (32) is then approximated as

$$p_f(t_0,t_s)=\frac{\sum_{i=1}^{N_s}I^+(l_{\max}(i))}{N_s} \tag{42}$$

where $I^+(l_{\max}(i))=1$ if $l_{\max}(i)>\beta$, otherwise, $I^+(l_{\max}(i))=0$.

It can be found from Eqs. (29) to (42) that only one MPP search is needed for reliability analysis under time-dependent random velocity field. The efficiency of the proposed method is therefore as good as that of time-independent reliabiity analsyis method.

6. EXAMPLE

6.1. Problem statement

In this section, a one-meter long steel turbine blade as shown in Fig. 8 is used to demonstrate the effectiveness of the proposed reliability analysis method. The turbine blade is twisted and has variable chord length along the radial direction. The airfoil used in this study case is the NREL S809 airfoil. The lift and drag coefficients of this airfoil are available in [53].

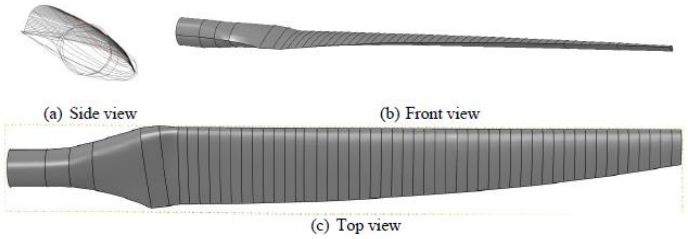

Fig. 8. Geometry configuration of the turbine blade

The other geometrical parameters, system parameters, and determnistic parameters for the velocity field model are given in Table 1.

Table 1. Parameters of the hydrokinetic turbine system

Variable	*D (m)*	*d (m)*	*R (m)*	*a*	*H (m)*
Value	0.1	0.15	1	0.85	7.5
Variable	v_h *(m/s)*	ω	n_r	ς $(^0)$	r_{root} *(m)*
Value	2.5	6.81	49	5	0.2

6.2. Reliability analysis

Following the procedure given in Sec. 2 through Sec. 5, we analyzed the time-dependent probability of failure of the

turbine blade over [0, 60] months (i.e. 5 years) using the proposed method. The results obtained from the proposed method are also compared with their counterparts from the brutal force Monte Carlo Simulation (MCS). For MCS, the time interval was divided into 60 time instants and 300 samples were generated at each time instant. There were therefore 18000 function evaluations of the FEA simulation for the MCS. The time-dependent probabilities of failure of the turbine blade over different time intervals are given in Table 2 and plotted in Fig. 9.

Table 2 Probabilities of failure over different time intervals

Time interval (months)	Proposed		MCS	
	p_f	ε (%)	p_f	95% CI
[0, 6]	0.25	15.60	0.21	[0.167, 0.260]
[0, 12]	0.35	1.42	0.35	[0.293, 0.401]
[0, 18]	0.43	7.57	0.46	[0.404, 0.516]
[0, 24]	0.48	1.89	0.49	[0.433, 0.547]
[0, 30]	0.52	3.43	0.54	[0.487, 0.600]
[0, 36]	0.56	1.12	0.57	[0.511, 0.623]
[0, 42]	0.59	0.21	0.59	[0.534, 0.646]
[0, 48]	0.61	0.87	0.62	[0.565, 0.675]
[0, 54]	0.64	0.66	0.64	[0.586, 0.694]
[0, 60]	0.66	0.67	0.66	[0.606, 0.714]

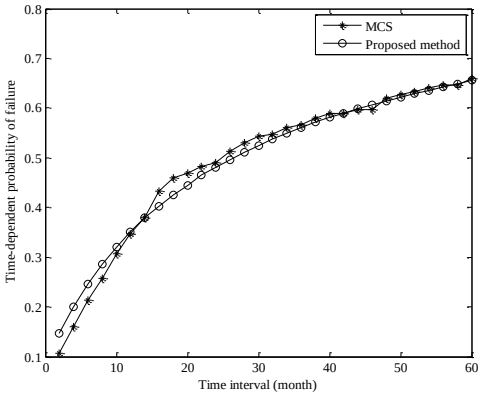

Fig. 9. Probabilities of failure over different time intervals

The results show that the accuracy of the proposed method is very good when compared with the benchmark of MCS. Even if there are some errors, the percentages of error are at acceptable levels. Table 3 gives the number of function calls and computational time needed by the proposed method and MCS for the time-dependent reliability analysis over [0, 60] months.

Table 3 Number of function calls for the proposed method and MCS over [0, 60] months

Method	Proposed	MCS
Function calls	28	18000

It indicates that the proposed method is much more efficient that MCS. It can save the computational time for time-dependent reliability analysis significantly. Fig. 10 presents the Cumulative Density Function (CDF) of the turbine blade under different limit states over the [0, 60] months. It illustrates that the proposed method is capable to accurately approximate the probability of failure of the turbine blade under different limit states. This has demonstrated the effectiveness of the proposed method in reliability analysis of the turbine blade.

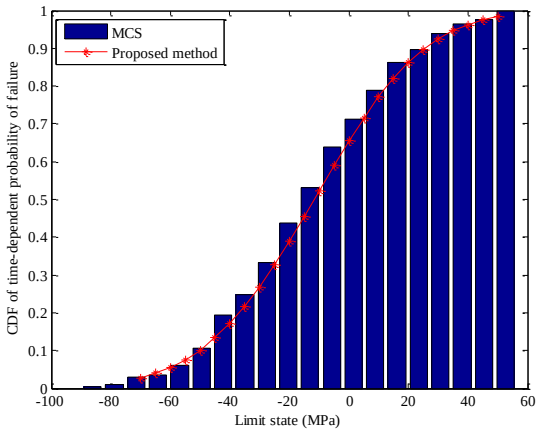

Fig. 18. Cumulative Density Function (CDF) of the limit state over [0, 60] months

From results of reliability analyses, it can be concluded that the proposed method is able to estimate the probability of failure of the turbine blade under time-dependent random velocity field efficiently and accurately. The proposed method therefore can be used to replace the computationally expensive MCS method during the design process of the turbine blade.

7. CONCLUSIONS

Reliability of the turbine blade is a vital issue that needs to be address during the development of hydrokinetic turbine system. The river velocity, which governs the load of hydrokinetic turbine blades, usually is expressed as a random variable without considering the correlations in space and time. In practical, it is more reasonable to describe the river velocity as a random field rather than a random variable. A reliability analysis method is developed in this work for the hydrokinetic turbine blade under random velocity field. The critical working position of the turbine blade is identified first based on the modeling of the velocity field and the blade element momentum (BEM) theory. The random velocity field is then constructed by introducing fluctuation part into the field model. To estimate the probability of failure of the turbine blade under different time intervals, a recently developed sampling approach for time-dependent reliability analysis method is integrated with the proper orthogonal decomposition (POD) method. The results of reliability analysis of a study case demonstrated that the accuracy and efficiency of the proposed method are good when compared with the benchmark of MCS. Considering that the proposed method is much more efficient than MCS, the method therefore can be employed to substitute MCS for the probabilistic design of the turbine blade in future.

In this work, the BEM theory is employed to analyze forces on the turbine blade given different velocity climates. In future, we will use the three dimensional computational fluid dynamics (CFD) simulations to more accurately capture the load environment of the turbine blade.

ACKNOWLEDGMENTS

This material is based upon work supported in part by the Office of Naval Research through contract ONR N000141010923 (Program Manager – Dr. Michele Anderson), the National Science Foundation through grant CMMI 1234855, and the Intelligent Systems Center (ISC) at the Missouri University of Science and Technology.

REFERENCE

[1] Elyakime, B., and Cabanettes, A., 2013, "Financial evaluation of two models for energy production in small French farm forests," Renewable Energy, 57, pp. 51-56.

[2] Kalkuhl, M., Edenhofer, O., and Lessmann, K., 2013, "Renewable energy subsidies: Second-best policy or fatal aberration for mitigation?," Resource and Energy Economics, 35(3), pp. 217-234.

[3] Mulder, M., and Scholtens, B., 2013, "The impact of renewable energy on electricity prices in the Netherlands," Renewable Energy, 57, pp. 94-100.

[4] Stoms, D. M., Dashiell, S. L., and Davis, F. W., 2013, "Siting solar energy development to minimize biological impacts," Renewable Energy, 57, pp. 289-298.

[5] Birjandi, A. H., Woods, J., and Bibeau, E. L., 2012, "Investigation of macro-turbulent flow structures interaction with a vertical hydrokinetic river turbine," Renewable Energy, 48, pp. 183-192.

[6] Kusakana, K., and Vermaak, H. J., 2013, "Hydrokinetic power generation for rural electricity supply: Case of South Africa," Renewable Energy, 55, pp. 467-473.

[7] Vanzwieten, J. H., Vanrietvelde, N., and Hacker, B. L., 2013, "Numerical simulation of an experimental ocean current turbine," IEEE Journal of Oceanic Engineering, 38(1), pp. 131-143.

[8] Yang, Z., Wang, T., and Copping, A. E., 2013, "Modeling tidal stream energy extraction and its effects on transport processes in a tidal channel and bay system using a three-dimensional coastal ocean model," Renewable Energy, 50, pp. 605-613.

[9] Yavuz, T., and Koç, E., 2012, "Performance analysis of double blade airfoil for hydrokinetic turbine applications," Energy Conversion and Management, 63, pp. 95-100.

[10] Ronold, K. O., and Larsen, G. C., 2000, "Reliability-based design of wind-turbine rotor blades against failure in ultimate loading," Engineering Structures, 22(6), pp. 565-574.

[11] Agarwal, P., 2008, "Structural reliability of offshore wind turbines," Ph.D Thesis, The University of Texas at Austin.

[12] Saranyasoontorn, K., and Manuel, L., 2004, "A comparison of wind turbine design loads in different environments using inverse reliability techniques," Journal of Solar Energy Engineering, Transactions of the ASME, 126(4), pp. 1060-1068.

[13] Saranyasoontorn, K., and Manuel, L., 2004, "Efficient models for wind turbine extreme loads using inverse reliability," Journal of Wind Engineering and Industrial Aerodynamics, 92(10), pp. 789-804.

[14] Hu, Z., and Du, X., 2012, "Reliability analysis for hydrokinetic turbine blades," Renewable Energy, 48, pp. 251-262.

[15] Val, D. V., and Chernin, L., "Reliability of tidal stream turbine blades," pp. 1817-1822.

[16] Hu, Z., Li, H., Du, X., and Chandrashekhara, K., 2012, "Simulation-based time-dependent reliability analysis for composite hydrokinetic turbine blades," Structural and Multidisciplinary Optimization, pp. 1-17.

[17] Delorm, T. M., Zappalà, D., and Tavner, P. J., 2012, "Tidal stream device reliability comparison models," Proceedings of the Institution of Mechanical Engineers, Part O: Journal of Risk and Reliability, 226(1), pp. 6-17.

[18] Saranyasoontorn, K., and Manuel, L., 2008, "On the propagation of uncertainty in inflow turbulence to wind turbine loads," Journal of Wind Engineering and Industrial Aerodynamics, 96(5), pp. 503-523.

[19] Sim, C., Basu, S., and Manuel, L., 2012, "On space-time resolution of inflow representations for wind turbine loads analysis," Energies, 5(7), pp. 2071-2092.

[20] Hu, W., Park, D., and Choi, D., 2013, "Structural optimization procedure of a composite wind turbine blade for reducing both material cost and blade weight," Engineering Optimization.

[21] Law, S. S., Bu, J. Q., and Zhu, X. Q., 2005, "Time-varying wind load identification from structural responses," Engineering Structures, 27(10), pp. 1586-1598.

[22] Chen, J. B., and Li, J., 2007, "The extreme value distribution and dynamic reliability analysis of nonlinear structures with uncertain parameters," Structural Safety, 29(2), pp. 77-93.

[23] Wang, Z., and Wang, P., 2012, "A nested extreme response surface approach for time-dependent reliability-based design optimization," Journal of Mechanical Design, Transactions of the ASME, 134(12).

[24] Chen, W., Tsui, K.-L., Allen, J. K., and Mistree, F., "Integration of the response surface methodology with the compromise decision support problem in developing a general robust design procedure," Proc. American Society of Mechanical Engineers, Design Engineering Division (Publication) DE 82 (1), pp. 485-492 pp. 485-492.

[25] Singh, A., Mourelatos, Z. P., and Nikolaidis, E., 2011, "An importance sampling approach for time-dependent reliability," Proceedings of the ASME Design Engineering Technical Conference, 2011, 5, pp. 1077-1088.

[26] Mori, Y., and Ellingwood, B. R., 1993, "Time-dependent system reliability analysis by adaptive importance sampling," Structural Safety, 12(1), pp. 59-73.

[27] González-Fernández, R. A., and Leite Da Silva, A. M., 2011, "Reliability assessment of time-dependent systems

via sequential cross-entropy Monte Carlo simulation," IEEE Transactions on Power Systems, 26(4), pp. 2381-2389.
[28] Breitung, K., 1984, "Asymptotic crossing rates for stationary Gaussian vector processes," Tech. Report, 1, Dept. of Math, and Statistics, Univ. of Lund, Lund, Sweden.
[29] Breitung, K., 1988, "Asymptotic approximations for the outcrossing rates of stationary vector processes," Stochast Process Appl, , 13, pp. 195–207.
[30] Andrieu-Renaud, C., Sudret, B., and Lemaire, M., 2004, "The PHI2 method: A way to compute time-variant reliability," Reliability Engineering and System Safety, 84(1), pp. 75-86.
[31] Xi, Z., Youn, B. D., and Hu, C., 2010, "Random field characterization considering statistical dependence for probability analysis and design," Journal of Mechanical Design, Transactions of the ASME, 132(10).
[32] Missoum, S., 2008, "Probabilistic optimal design in the presence of random fields," Structural and Multidisciplinary Optimization, 35(6), pp. 523-530.
[33] Basudhar, A., and Missoum, S., 2009, "A sampling-based approach for probabilistic design with random fields," Computer Methods in Applied Mechanics and Engineering, 198(47-48), pp. 3647-3655.
[34] Biegel, B., Juelsgaard, M., Kraning, M., Boyd, S., and Stoustrup, J., "Wind turbine pitch optimization," Proc. 2011 20th IEEE International Conference on Control Applications, pp. 1327-1334.
[35] Smart, G. M., 1999, "Turbulent velocity profiles and boundary shear in gravel bed rivers," Journal of Hydraulic Engineering, 125(2), pp. 106-116.
[36] Dolan, D. S. L., and Lehn, P. W., 2006, "Simulation model of wind turbine 3p torque oscillations due to wind shear and tower shadow," IEEE Transactions on Energy Conversion, 21(3), pp. 717-724.
[37] Martin, O. L. H., 2008, Aerodynamics of wind turbines, Second edition, Earthscan, Sterling, VA.
[38] Manwell, J. F., J. G. McGowan 2002, Wind Energy Explained: Theory, Design and Application. New York, John Wiley and Sons.
[39] Diazdelao, F. A., and Adhikari, S., 2011, "Gaussian process emulators for the stochastic finite element method," International Journal for Numerical Methods in Engineering, 87(6), pp. 521-540.
[40] Liu, P. L., and Der Kiureghian, A., 1986, "Multivariate distribution models with prescribed marginals and covariances," Probabilistic Engineering Mechanics, 1(2), pp. 105-112.
[41] Li, C.-C., and Der Kiureghian, A., 1993, "Optimal discretization of random fields," Journal of Engineering Mechanics, 119(6), pp. 1136-1154.
[42] Keating, J. P., Michalek, J. E., and Riley, J. T., 1983, "A note on the optimality of the Karhunen-Loeve expansion," Pattern Recognition Letters, 1(4), pp. 203-204.
[43] Kirby, M., and Sirovich, L., 1990, "Application of the Karhunen-Loeve procedure for the characterization of human faces," IEEE Transactions on Pattern Analysis and Machine Intelligence, 12(1), pp. 103-108.
[44] Watanabe, S., 1981, "Pattern recognition as a quest for minimum entropy," Pattern Recognition, 13(5), pp. 381-387.
[45] Wornell, G. W., 1990, "Karhunen-Loeve-like expansion for 1/f processes via wavelets," IEEE Transactions on Information Theory, 36(4), pp. 859-861.
[46] Der Kiureghian, A., and Ke, J. B., 1988, "The stochastic finite element method in structural reliability," Probabilistic Engineering Mechanics, 3(2), pp. 83-91.
[47] Sudret, B., and Der Kiureghian, A., 2002, "Comparison of finite element reliability methods," Probabilistic Engineering Mechanics, 17(4), pp. 337-348.
[48] Manuel, L., Veers, P. S., and Winterstein, S. R., 2001, "Parametric models for estimating wind turbine fatigue loads for design," Journal of Solar Energy Engineering, Transactions of the ASME, 123(4), pp. 346-355.
[49] Saranyasoontorn, K., and Manuel, L., "On the study of uncertainty in inflow turbulence model parameters in wind turbine applications," pp. 16429-16442.
[50] Shumway., R. H., and Stoffer, D. S., 2009, Time series analysis and its applications, Springer, New York.
[51] Hu, Z., and Du, X., 2013, "First Order Simulation for Time Dependent Reliability," ASME Journal of Mechanical Design, Submitted.
[52] Zhang, J., and Ellingwood, B., 1994, "Orthogonal series expansions of random fields in reliability analysis," Journal of Engineering Mechanics, 120(12), pp. 2660-2677.
[53] David J. Laino, A. C. H., 2002, "National Renewable Energy Laboratory Report, Report Number: NREL/TP-442-7817 Appendix B."